

Article

Mapping Fine Spatial Resolution Precipitation from TRMM Precipitation Datasets Using an Ensemble Learning Method and MODIS Optical Products in China

Xiaodan Zhao ^{1,2,3}, Wenlong Jing ^{1,2,3,*}  and Pengyan Zhang ^{4,*}

¹ Guangzhou Institute of Geography, Guangzhou 510070, China; zhaoxd@reis.ac.cn

² Key Laboratory of Guangdong for Utilization of Remote Sensing and Geographical Information System, Guangzhou 510070, China

³ Guangdong Open Laboratory of Geospatial Information Technology and Application, Guangzhou 510070, China

⁴ College of Environment and Planning, Henan University, Kaifeng 475004, China

* Correspondence: jingwl@reis.ac.cn (W.J.); pengyanzh@henu.edu.cn (P.Z.)

Received: 13 September 2017; Accepted: 19 October 2017; Published: 23 October 2017

Abstract: Precipitation data are important for the fields of hydrology and meteorology, and are fundamental for ecosystem monitoring and climate change research. Satellite-based precipitation products are already able to provide high temporal resolution precipitation information at a global level. However, the coarse spatial resolution has restricted their use in regional level studies. In this study, monthly fine spatial resolution land precipitation data in China was obtained by downscaling the TRMM 3B43 V7 monthly precipitation products. The downscaling model was constructed based on the ensemble learning method called random forest (RF). In addition to the RF model, the classification and regression tree (CART) model was also used to downscale the precipitation data for the purpose of comparison. The results were validated with in situ measurements. Results showed that the RF model outperformed the CART model. The downscaled precipitation data were strongly correlated with the in situ measurements. The downscaling method was applied to mapping fine spatial resolution precipitation over all of China, and is valuable for developing high spatial resolution precipitation products for studies on hydrology, meteorology, and climate science.

Keywords: precipitation; spatial downscaling; Tropical Rainfall Measuring Mission; China

1. Introduction

Precipitation is a key component of the global water cycle [1–7], and is important for plant physiological, ecological, environmental, and hydrological models [8–11]. Mapping precipitation with high spatial resolution is therefore beneficial for monitoring ecosystem and environmental changes. Satellites with radar and microwave sensors can provide reliable sources of precipitation data [3,5,12–16], especially for un-gauged regions. During the past three decades, a multitude of global precipitation products have been published and they were widely used in multiple hydrological, meteorological, and environmental applications [3,14,17,18]. These products were mainly estimated by integrating remotely sensed microwave (MW) and infrared (IR) data. The precipitation radar launched by the Tropical Rainfall Measuring Mission (TRMM) was the first satellite-based active MW sensor designed for precipitation detection and it provided reliable precipitation estimation for the tropical and mid-latitudes [19]. Those precipitation products are fundamental for many global scale models and applications, but typically are not suitable for regional applications due to their coarse spatial resolution [20,21].

The development of spatial downscaling techniques can address this problem by improving the spatial resolution of images or gridded datasets. Spatial downscaling methods are helpful for obtaining fine spatial resolution precipitation data from coarse resolution precipitation products. Various approaches have been developed to downscale satellite-based precipitation by integrating the impact of several environmental variables. These methods seek to establish a statistical correlation model between coarse resolution precipitation datasets and fine resolution auxiliary variables. Precipitation is a continuous variable, so linear regression algorithms have been used in downscaling models for fitting the relationship between precipitation and other variables [20–23]. In addition, various methods, such as machine learning and the interpolation approach, have been implemented to fill gaps in climatic variables, such as streamflow, total water storage changes, air temperature, and soil moisture [24–27]. However, these methods have not been widely used for downscaling satellite-based precipitation datasets. The ensemble learning method is defined as a type of learning algorithm that uses multiple predictors to produce a more accurate prediction. The basic principle of ensemble learning methods is to construct a more robust learner by grouping a number of individual learners. Fast algorithms, such as classification and regression tree (CART), are commonly used as the basic predictor in ensemble methods. The random forest (RF) is a popular ensemble learning method and has been reported to have good performance for a variety of applications [28]. In addition, RF can efficiently handle large datasets. Precipitation is difficult to simulate and estimate with simple statistical algorithms due to its own complexity and the complex relationship with other factors. In this study, we used the RF algorithm to construct the downscaling model to evaluate its potential value in mapping fine spatial resolution precipitation products.

The aims of this study were threefold: (1) to downscale the TRMM 3B43 V7 monthly precipitation products from a spatial resolution of 25 km to 1 km; (2) to evaluate the performance of the CART and RF algorithm in downscaling satellite-based precipitation products; and (3) to generate fine spatial resolution precipitation products for China.

2. Study Area and Data Resources

2.1. Study Area

This downscaling study was conducted for China land area. Its latitudes range from 18° N to 54° N, and longitudes range from 73° E to 135° E. A marked continental monsoonal climate dominates the most part of China. Because of complex terrain and wide area, precipitation and temperature conditions vary extremely from west to east and from south to north [29,30]. Figure 1 shows the topography and the spatial distribution of the 675 meteorological stations in China. According to Figure 1, ground-based weather networks are sparse in western China due to harsh natural conditions, the satellite-based precipitation datasets, therefore, are significant for hydrological and environmental studies over these regions.

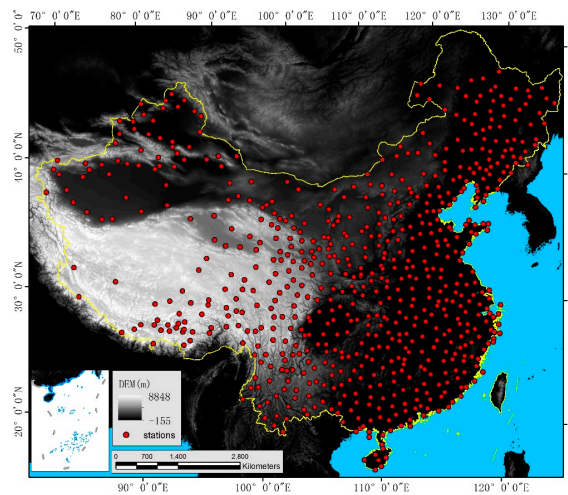


Figure 1. Map of the elevation and 675 meteorological stations in China.

2.2. Data Sources

The TRMM satellite, launched in late November 1997, has provided multiple precipitation products for more than 17 years. The TRMM-based precipitation products have good performance and have been the standard for the validation of other satellite-based precipitation products because of their reliable quality [15]. In this study, the products used for were version 7 of the TRMM 3B43 monthly precipitation product for 2003, 2006, and 2009. The TRMM 3B43 V7 products are produced at a spatial resolution of $0.25^\circ \times 0.25^\circ$, covering 50°N – 50°S . The original TRMM 3B43 V7 data were re-projected to the Albers Conical Equal Area projection and resampled to 25 km resolution using the nearest neighbor resampling algorithm during the re-projection.

Two Moderate Resolution Imaging Spectroradiometer (MODIS) optical products, monthly NDVI (MOD13A3) and daily land surface temperature (MOD11A1), with 1 km spatial resolution were jointly used to downscale the TRMM precipitation products. Monthly LST was calculated by averaging daily land surface temperature (LST) in corresponding months. The digital elevation model (DEM) dataset used in this study was from the Shuttle Radar Topographic Mission (SRTM). The SRTM DEM with 1 km spatial resolution was downloaded from the website <http://glcf.umd.edu/data/srtm/>.

For validation purposes, the ground-based monthly climate variables dataset of China were used. The dataset includes 675 weather stations over China land area (Figure 1), it provides in situ measured monthly total precipitation. The original dataset are obtained from China Meteorological Data Service Center (CMDC) (<http://data.cma.cn/en/>).

3. Methods

3.1. Downscaling Algorithm

The spatial downscaling algorithm for mapping precipitation at high spatial resolution from TRMM 3B43 V7 precipitation products, using MODIS-derived NDVI and LST products, consisted of two main steps which are described as follows. A flowchart showing the main steps of the process is presented in Figure 2.

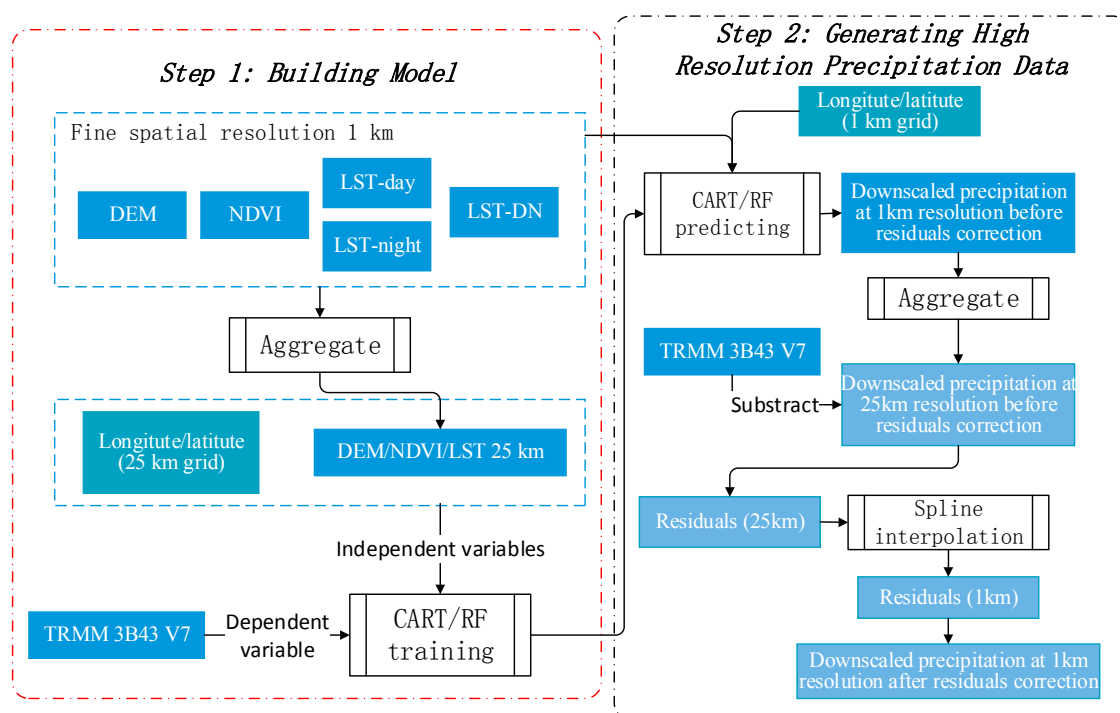


Figure 2. Process used for generating fine spatial resolution precipitation data.

The first step involved building the model. A precipitation estimation model, based on the relationship between precipitation and environmental variables, was developed. The CART and RF algorithm were used to establish the downscaling model at a grid pixel resolution of 25 km by 25 km. Multiple studies have acknowledged that precipitation data are strongly correlated to NDVI, LST, and DEM [31–35]. As precipitation is a spatially heterogeneous variable, geolocations (longitude and latitude) are also considered variables that reflect spatial variations in precipitation.

There were seven inputs for the downscaling model: NDVI, daytime LST (LST_{day}), nighttime LST (LST_{night}), day–night LST difference (LST_{DN}), DEM, longitude, and latitude. First, the NDVI, LSTs, and DEM were aggregated to 25 km using an averaging algorithm. Then, the CART and RF models were both trained at a grid cell of 25 km by 25 km.

The second step involved generating high resolution precipitation data. Precipitation maps at a resolution of 1 km (PRCP1km) were obtained by applying the models in the first step to original MODIS optical products and DEM data at 1 km. Then, a residual correction was performed on the PRCP1km maps that the model could not estimate. The residual correction includes three steps: (1) The PRCP1km were aggregated to coarse spatial resolution (25 km) using an averaging method. The residuals were then calculated by subtracting the re-sampled PRCP1km from the original TRMM products. (2) The coarse resolution residuals were spatially interpolated to mapping residuals at fine resolution (1 km); a spline interpolation method was implemented here for its usefulness for regularly-spaced data [20,21]. (3) The residuals at 1 km resolution were then added back to PRECP1km. Lastly, the overcorrected values (negative values) were replaced by zero to guarantee a reasonable range of the downscaled precipitation data.

3.2. Random Forests

Ensemble learning is a method that uses a number of individual predictors to obtain better quality predictions. In theory, it performs better than any single predictor. Random forest (RF) is a well-known ensemble learning method that has been widely used for both classification and regression, and was reported to outperform a number of machine learning algorithms. The RF was developed

by Breiman [36]. It constructs a multitude of classification and regression trees (CART) by randomly extracting subsets from the total dataset with replacement. For classification problems, the final output is the mode of the classes of all the individual trees. For regression problems, the predicted results are obtained by averaging the predictions of the individual trees. The basic process of RF regression method can be described as follows: (1) The total number (N) of subsets is extracted randomly from the total sample set with replacement; (2) For each subset, a regression tree is generated. All of the trees are constructed independently. In each tree, a number of random variables are selected at a root node of the tree and the best variable split is selected in order to split the node into two sub-nodes; (3) The predictions are obtained by averaging the prediction of each individual trees:

$$f = \frac{1}{N} \sum_{i=1}^N f_i(x) \quad (1)$$

where N is the number of trees and $f_i(x)$ is the prediction from each individual regression tree.

For comparison in this study, the CART model was used to downscale the TRMM precipitation products. Further details about CART and RF algorithm are provided in Breiman [36] and Breiman et al. [37].

4. Results and Analysis

4.1. Performance of the Regression Algorithms

The CART and RF models were trained on a 25 km by 25 km scale. Optimization of model parameters are significant for utility of machine learning algorithms. In practice, we optimized parameters to obtain the best training performance by introducing a grid search algorithm (GS). The basic idea of GS is to traversal the pre-set parameter sets to find the best training accuracy based on cross-validation (CV). In this study, we used a CV scheme that divide the total dataset into three subsets randomly; two subsets are used for learning, and the left one is used for testing. The candidate parameters used can be seen in Table 1.

Table 1. Candidate parameters for classification and regression trees (CART) and random forest (RF).

Algorithm	Parameter Type	Description of Parameter Type	Parameters
Classification and Regression Trees	MinSamplesLeaf	The minimum number of samples required to split an internal node.	2, 3, 4, 5, 6, 7, 8, 9, 10
Random Forests	n_estimators	The number of trees in the forest	20, 40, 60, 80, 100, 120, 140, 160, 180, 200, 220, 240, 260, 280, 300

By using the grid search algorithm, we derived the coefficient of determination (R^2) achieved by the training models with different parameters (Figure 3). As shown in Figure 3, the R^2 values between the predictor and the target obtained by the CART model varied between 0.90 and 0.99 when the parameters were changed. In contrast, the RF model produced more stable R^2 values with different parameters; the averaged R^2 values were all higher than 0.99. In general, the RF model performed better than the CART model when establishing the downscaling model. According to the analysis above, the performance of RF model is stable when the 'n_estimators' changes; in addition, the RF model has good robustness compared to the CART model. However, as 'n_estimators' decreases, the strength of the RF model tends to decrease as well. Selecting appropriate parameters for different datasets and application scenarios is needed.

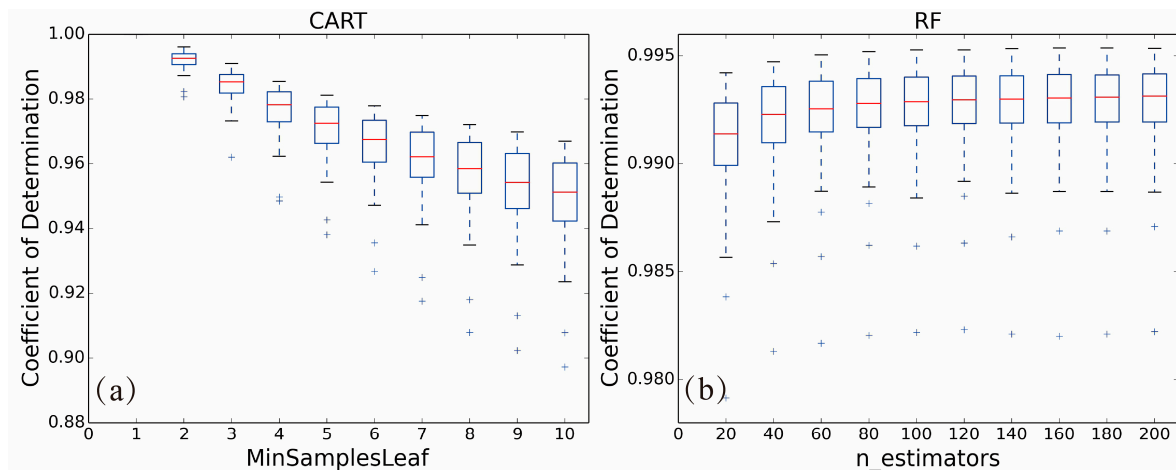


Figure 3. Coefficient of determination of the two algorithms: (a) CART and (b) RF.

4.2. Mapping Fine Spatial Resolution Precipitation

By applying the CART and RF models to variables at a fine spatial resolution of one kilometer, we generated fine spatial resolution precipitation data over China's land area. Figure 4 shows the original TRMM products in May 2009 (Figure 4a) and the fine spatial resolution precipitation maps generated using the CART and RF models separately. Through visual comparison, the results generated by the two models show similar spatial distribution patterns. We then compared the scatter plots between the original and the aggregated fine spatial resolution precipitation maps (Figure 5). The precipitation map generated using the RF model has a higher correlation with the original TRMM products than those obtained by the CART model, as shown in Figure 5.

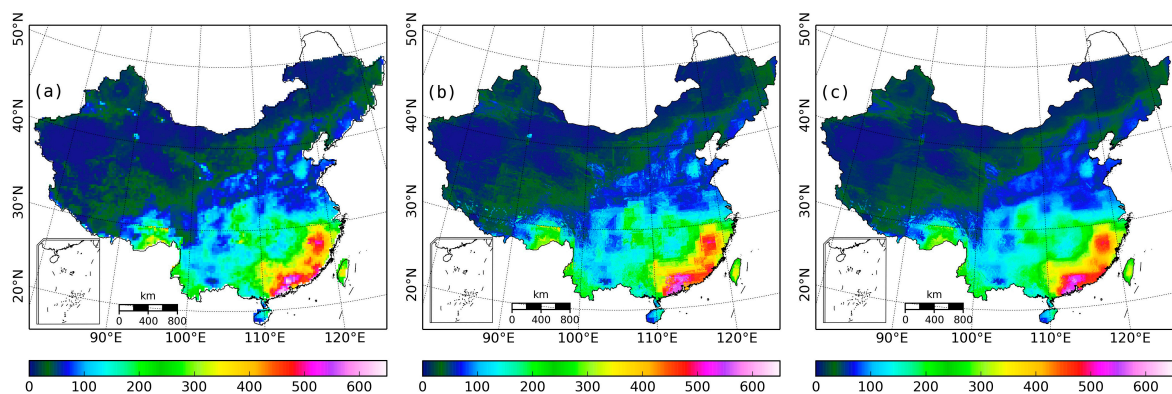


Figure 4. (a) Tropical Rainfall Measuring Mission (TRMM) 3B43 V7 precipitation products and the downscaled precipitation maps without residual correction created with (b) CART and (c) RF in May 2009.

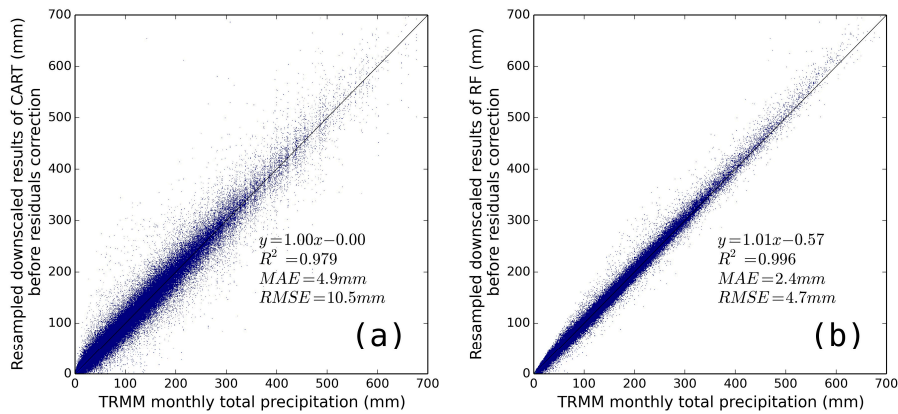


Figure 5. The scatter plots between the original TRMM 3B43 V7 precipitation and resampled downscaled precipitation maps without residual correction for (a) CART and (b) RF.

The fine spatial resolution precipitation maps generated by the CART and RF models were then corrected by using the residual correction method described above to produce final downscaled precipitation. Figures 6 and 7 present the corrected precipitation maps for the same time period and the scatter plots between the corrected precipitation and TRMM products. The results of the CART model were improved by the correction, while the RF model preserved the properties of the original TRMM data perfectly, both before and after residual correction.

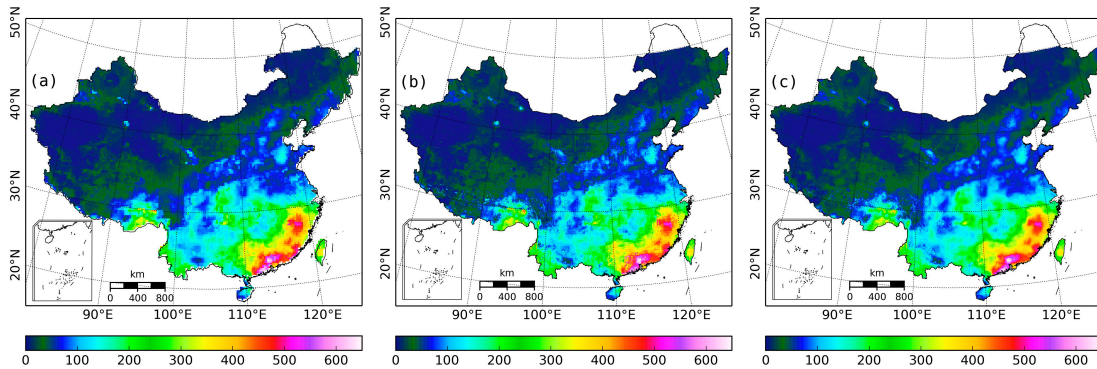


Figure 6. (a) TRMM 3B43 V7 precipitation products and downscaled precipitation maps after residual correction with (b) CART and (c) RF in May 2009.

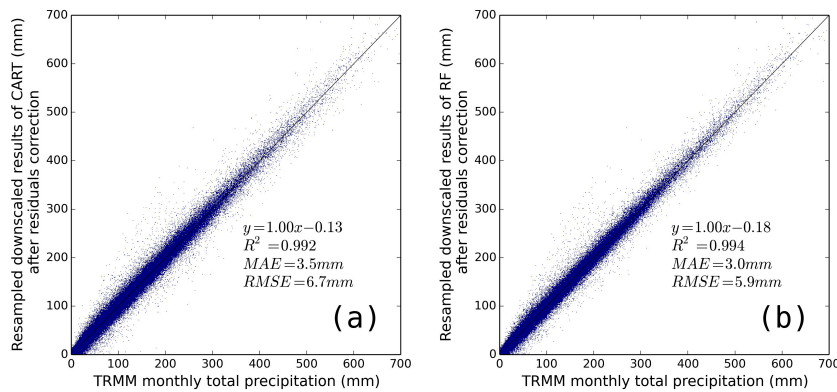


Figure 7. The scatter plots between the original TRMM 3B43 V7 precipitation data and resampled downscaled results after residual correction with (a) CART and (b) RF.

Figure 8 illustrates the effectiveness of the developed approach for downscaling precipitation in July 2006 for the TRMM precipitation products. Figure 8c,e highlight the downscaled precipitation maps created by the RF model for different areas. The coarse resolution precipitation data appear to be downscaled well. The downscaled precipitation map could provide more spatial details within each coarse grid. Fine spatial resolution precipitation products could strengthen the potential of satellite-based precipitation products for regional applications.

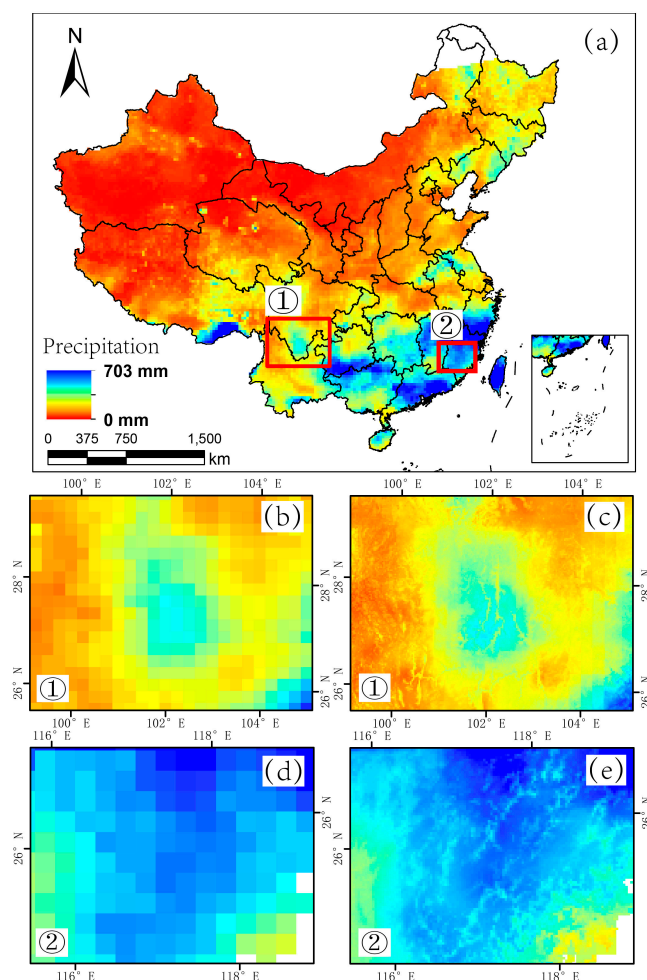


Figure 8. (a) TRMM 3B43 precipitation map of China in July 2006 and the indicator boxes for the two areas; (b) TRMM precipitation map of area ① in July 2006; (c) downscaled precipitation map of area ① in July 2006; (d) TRMM precipitation map of area ② in July 2006; and (e) downscaled precipitation map of area ② in July 2006.

4.3. Validation and Analysis

4.3.1. Validation for In Situ Measurements

The downscaled results were analyzed using in situ measurements for validation. First, we validated the downscaled precipitation data before residual correction, and the results are shown in Figure 9. The CART model estimated the precipitation with an R^2 value of 0.74. Compared with CART, the RF model had a higher R^2 , and a smaller mean absolute error (MAE) and root-mean-square error (RMSE). The residual corrected precipitation data were then validated with in situ measurements (Figure 10). Compared to the precipitation without correction, the corrected precipitation data had a higher R^2 value and a smaller MAE and RMSE. We examined the performance of the final

downscaled precipitation data for different months. Table 2 presents the validation results with in situ measurements. In general, the RF model performed better than the CART model in each month, with higher R^2 values and smaller MAE and RMSE values.

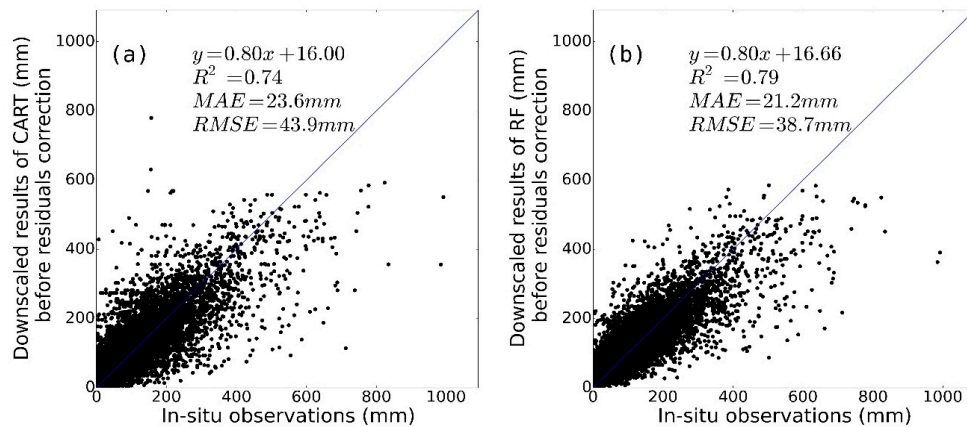


Figure 9. The scatter plots comparing the in situ observations and downscaled precipitation without correction using (a) CART and (b) RF.

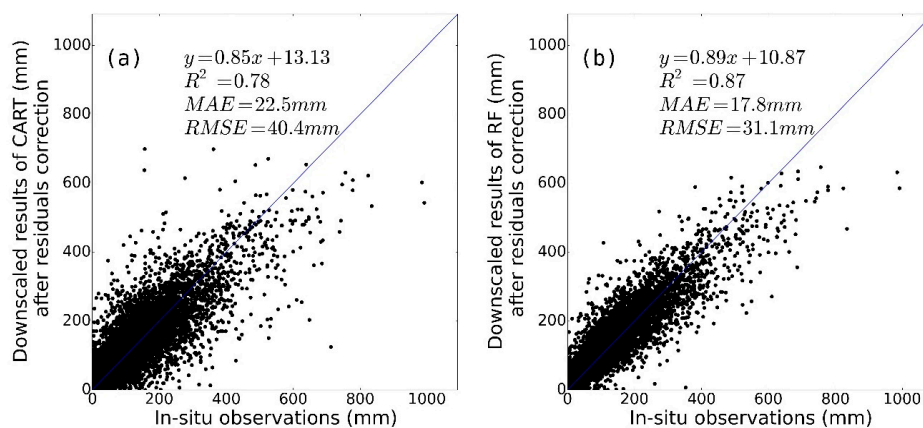


Figure 10. The scatter plots comparing the in situ observations and downscaled precipitation after correction using (a) CART and (b) RF.

Table 2. The coefficient of determination (R^2), mean absolute error (MAE), and root-mean-square error (RMSE) of each algorithm for different months.

Month	CART			RF		
	R^2	MAE (mm)	RMSE (mm)	R^2	MAE (mm)	RMSE (mm)
1	0.822	5.6	9.8	0.823	5.4	9.4
2	0.851	9.0	16.8	0.882	8.2	15.0
3	0.862	11.3	20.0	0.892	10.2	17.5
4	0.811	19.3	30.4	0.862	16.7	25.4
5	0.835	24.8	38.3	0.869	21.5	34.1
6	0.766	36.5	55.2	0.804	33.1	50.4
7	0.566	48.8	73.5	0.655	41.8	62.9
8	0.620	41.1	61.8	0.699	36.0	54.1
9	0.670	26.6	40.9	0.738	23.2	36.2
10	0.666	17.1	28.9	0.736	15.0	24.9
11	0.809	10.9	17.7	0.848	9.8	15.8
12	0.738	5.6	9.5	0.774	5.1	8.7

A zoning system divides the land area of China into nine regions. The zones were determined based on regional similarities and differences in precipitation, temperature, terrain, conditions, and potential for development of agricultural production. It was published by the National Committee of Agricultural Regionalization under the State Agricultural Commission of China [38,39]. This zoning system facilitates the analysis of changes and differences in precipitation and temperature between locations. The topography, land cover type, and ecosystems of different regions can greatly vary. The downscaled precipitation data in different regions were analyzed with in situ precipitation based on the zoning system. The nine regions are identified as R_i where i ranges from one to nine (Figure 11). Figures 12 and 13 present the scatter plots comparing the in situ observations and the final downscaled precipitation maps created with CART and RF. In general, the RF model performed better than the CART model in each region. However, both the CART and RF models had small R^2 values and high bias in R8.

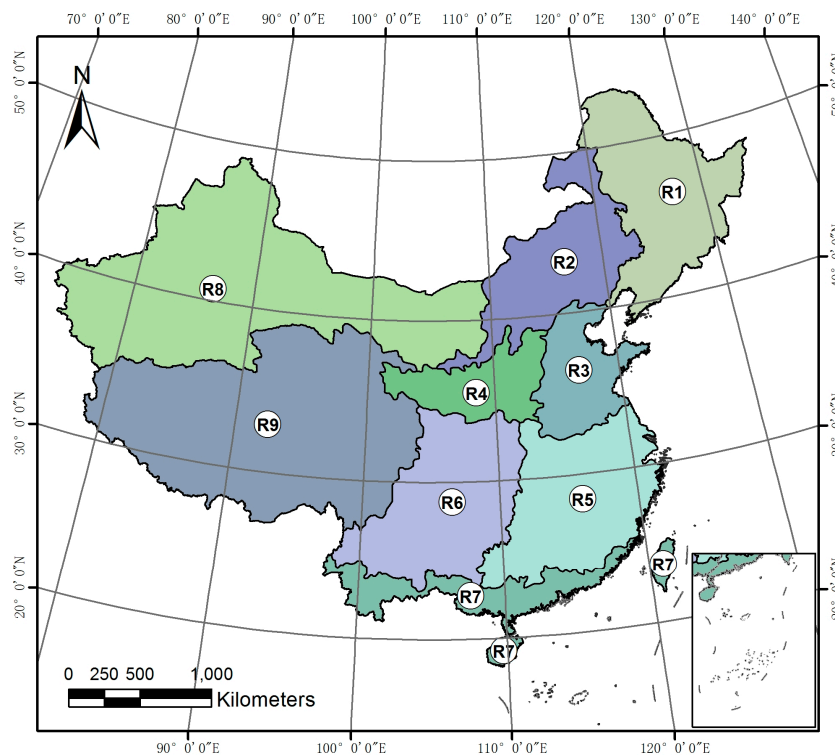


Figure 11. The zoning system that divides the land area of China into nine regions.

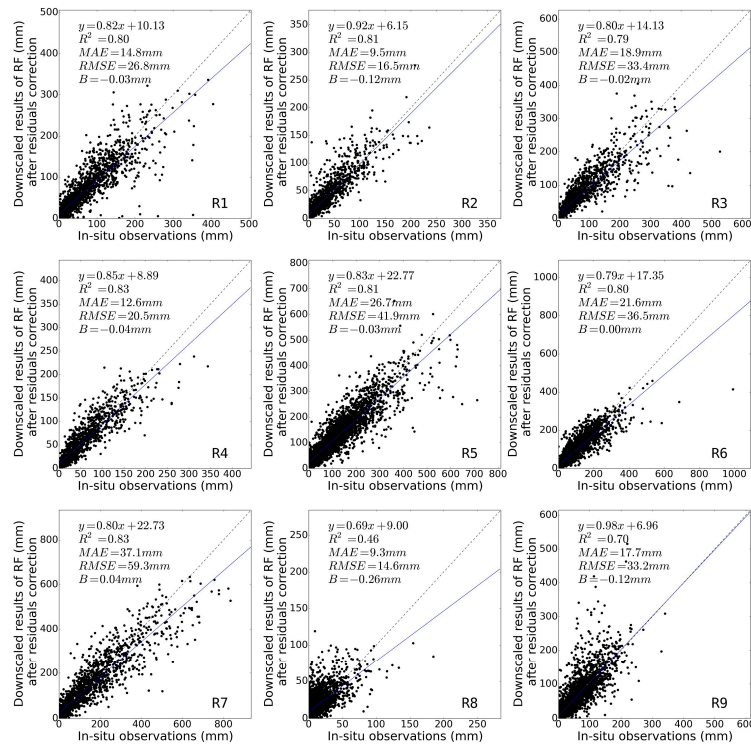


Figure 12. The scatter plots comparing the in situ observations and the downsampled precipitation data using the CART model.

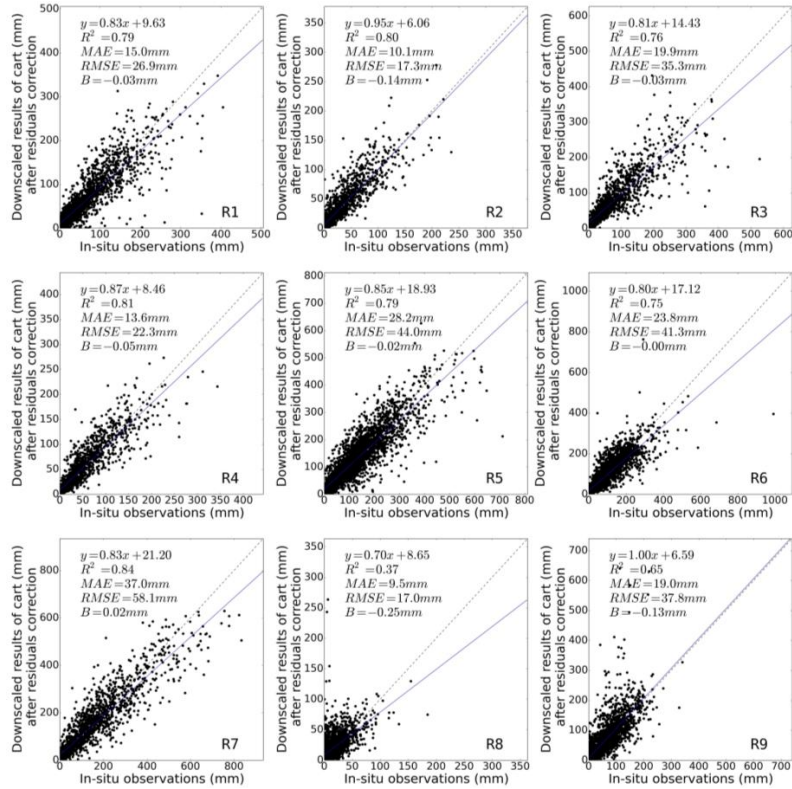


Figure 13. The scatter plots comparing in situ observations and the downsampled precipitation data created with the RF model.

The temporal behavior of the downscaled precipitation data was then examined. Figure 14 shows the comparison of the station-averaged in situ precipitation data and the station-averaged downscaled precipitation data for each region during the time period. In general, the precipitation products accurately captured the precipitation dynamics. For R8, the downscaled results generally overestimated precipitation compared with the in situ measurements. The precipitation products significantly overestimated precipitation in the summer months of June, July, and August in R9.

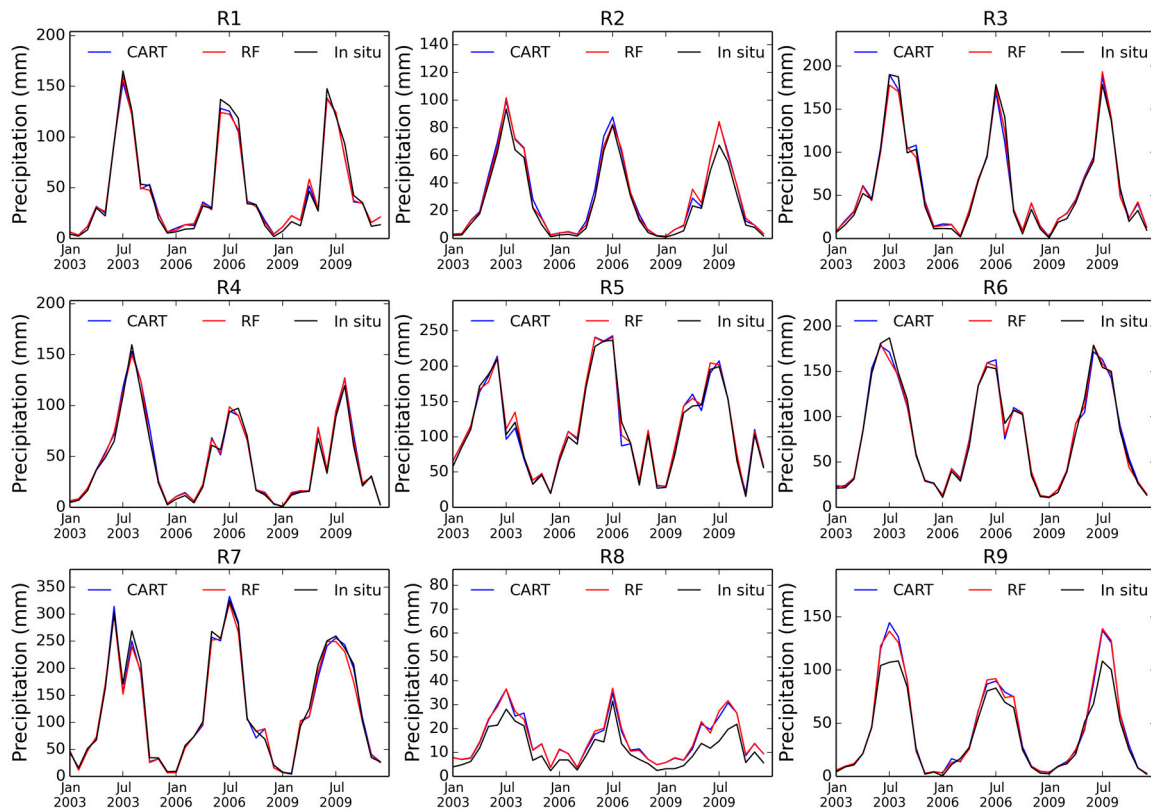


Figure 14. Comparison of station-averaged in situ measurements and downscaled precipitation for each region.

4.3.2. Error Analysis

We analyzed the errors in the downscaled precipitation data. First, we compared the station-averaged mean absolute error (MAE) with the in situ average precipitation data (Figure 15). Results showed that MAE was positively correlated to the precipitation. As illustrated in Figure 15, the MAE of the downscaled precipitation data obtained by CART increased at a rate of 2.7 mm/10 mm ($R^2 = 0.62$), whereas the RF model had a smaller trend of 2.4 mm/10 mm. We further investigated the relationship between the accuracy of the original TRMM products and the performance of the downscaled results to determine the sources of the errors. The accuracy of the TRMM products and the downscaled precipitation were assessed by comparing the MAE of the in situ measurements and the precipitation datasets. Figure 16 shows the scatter plots of the MAE of the TRMM and the downscaled results. The MAE of the monthly precipitation datasets obtained by the RF model has a strong relationship with that of the original TRMM data, with an R^2 value of 0.89. This indicates that the accuracy of the downscaled precipitation data may be strongly affected by the accuracy of the original satellite precipitation datasets.

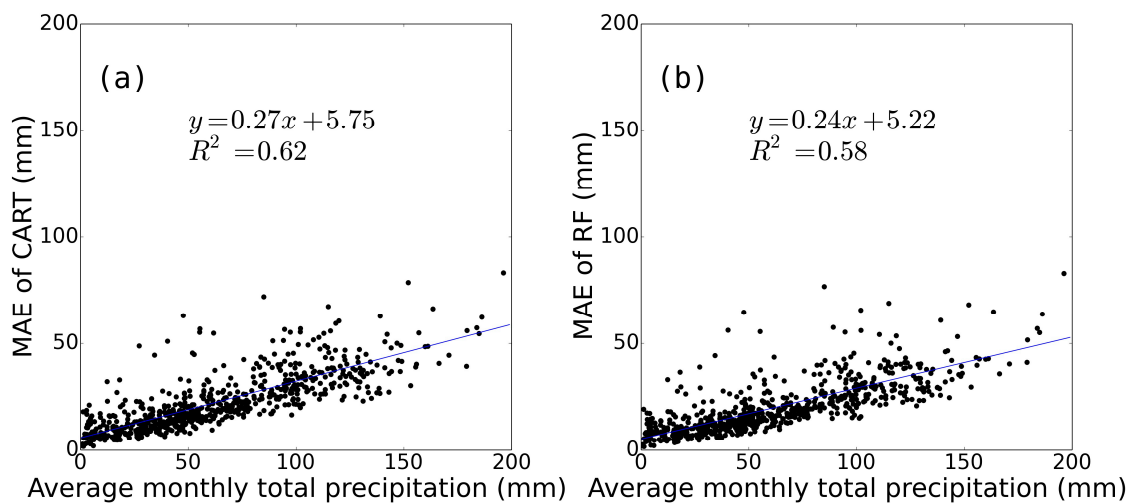


Figure 15. Scatter plots showing the average MAE of the downscaled results obtained by using (a) CART and (b) RF, and the arithmetic mean of the observed precipitation for each station.

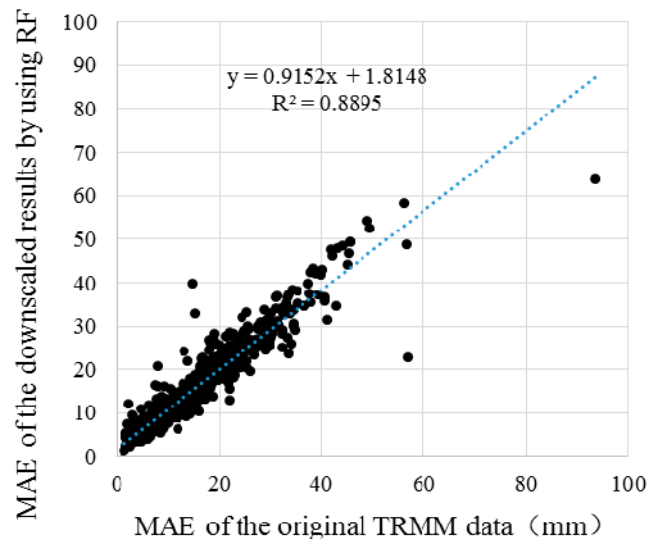


Figure 16. Scatter plots of the MAE of the original TRMM data and the MAE of the results obtained by using the RF-based model.

5. Discussion

Investigating changes and spatial variations in precipitation is important to better understand global climate change and its impact on regional ecosystems. Satellite-based precipitation observations are valuable resources for climate change, hydrological simulation, and drought and flood monitoring. However, the coarse spatial resolution of the satellite-based precipitation products reduces the potential for regional uses.

To address the limitation on regional applications imposed by this coarse spatial resolution, we generated fine spatial resolution precipitation datasets from a satellite-based (TRMM 3B43 V7) precipitation product by using a RF-based downscaling method and optical remote sensing products. The downscaling approach depends mainly on NDVI, LST, and DEM. These variables have been investigated and proven to be strongly related to precipitation changes and spatial distribution [40–46]. However, several human and natural variables affect this relevance, which as a result, reduce the potential of using these variables as indicators in downscaling precipitation data for certain areas.

For instance, irrigation and harvesting processes can influence the NDVI and LST values of farmland, and the defoliation of vegetation would also change these values of these variables [22]. These non-precipitation effects on the variation in NDVI and LST might result in some uncertainty in precipitation downscaling. This uncertainty was not evaluated in this study. These influences need to be explored to reduce the uncertainties in future work. In addition, the distribution of the stations is uneven and sparse in the western Tibetan Plateau (TP) due to the high altitude, the complex topographical conditions, and the extremely cold climatic conditions [45,47,48]. Therefore, uncertainties in the regional trends would arise because of a lack of reliable data. These uncertainties in the downscaled precipitation dataset over the west TP area were not analyzed because of the lack of ground-based observations.

According our analysis in Section 4.3.2, the performance of the downscaled precipitation dataset is greatly affected by the accuracy of the original precipitation products. Previous studies have found that the TRMM-based precipitation datasets have limited ability to estimate solid precipitation, which is the main form of precipitation over the middle and high latitudes in winter [22]. Thus, uncertainty may arise in the data during winter in these regions.

6. Conclusions

Fine spatial resolution precipitation datasets are useful for characterizing the details of the spatial distribution of precipitation, and are helpful to bridge the gap between coarse spatial resolution precipitation and their application to regional studies. Land surface temperature was combined here with NDVI and DEM data to downscale the TRMM 3B43 V7 precipitation datasets in China from a resolution of 25 km to 1 km using the CART and RF models. The coherence and accuracy of the results were validated and verified based on the actual data from meteorological stations.

The verification results indicated the RF model had higher coherence and precision than the CART model, both before and after residual correction. The RF model performed well in downscaling the precipitation datasets and achieved results with high accuracy for every month. Moreover, we observed a relatively significant positive and linear correlation between the estimated errors and the average observed precipitation. In addition, the rates of the RF-based model are lower than the CART-based model.

We recommend that researchers introduce more precipitation correlated features, such as soil moisture, slope, and aspects, to determine if they are valuable variables for downscaling satellite precipitation data in a subsequent study. Furthermore, the TRMM mission ended in 2015; the next generation precipitation products of Precipitation Measurement Missions (GPM) have higher spatial and temporal resolution. Moreover, we recommend that future studies focus on exploring downscaling algorithms for weekly or daily precipitation datasets, which would be more valuable for hydrological, meteorological, and ecological research.

Acknowledgments: This study was jointly supported by the GDAS' Special Project of Science and Technology Development (2017GDASCX-0101, 2018GDASCX-0904), Guangdong Innovative and Entrepreneurial Research Team Program (2016ZT06D336), the National Natural Science Foundation of China (41601175, 41401430), the key scientific research project of Henan province (16A610001), the Foundation and Advanced Technology Research Plan of Henan Province (152300410067), the Program for Innovative Research Team (in Science and Technology) in University of Henan Province (16IRTSTHN012), the Opening Fund of Henan Key Laboratory of Integrated Air Pollution Control and Ecological Security(20170201), and the National Earth System Science Data Sharing Infrastructure (<http://www.geodata.cn/>). We appreciated the National Aeronautics and Space Administration (NASA) for providing us with the access to acquire the MODIS, TRMM, and DEM data that were utilized in this study.

Author Contributions: Xiaodan Zhao drafted the manuscript and was responsible for the research design, experiment, and analysis. Pengyan Zhang and Wenlong Jing reviewed the manuscript and were responsible for the research design and analysis. All of the authors contributed to editing and reviewing the manuscript.

Conflicts of Interest: The authors declare no conflict of interest.

References

1. Taylor, C.M.; de Jeu, R.A.M.; Guichard, F.; Harris, P.P.; Dorigo, W.A. Afternoon rain more likely over drier soils. *Nature* **2012**, *489*, 423–426. [[CrossRef](#)] [[PubMed](#)]
2. Sapiiano, M.R.P.; Arkin, P.A. An intercomparison and validation of high-resolution satellite precipitation estimates with 3-hourly gauge data. *J. Hydrometeorol.* **2009**, *10*, 149–166. [[CrossRef](#)]
3. Kubota, T.; Shige, S.; Hashizume, H.; Aonashi, K.; Takahashi, N.; Seto, S.; Hirose, M.; Takayabu, Y.N.; Ushio, T.; Nakagawa, K.; et al. Global precipitation map using satellite-borne microwave radiometers by the gsmmap project: Production and validation. *IEEE Trans. Geosci. Remote Sens.* **2007**, *45*, 2259–2275. [[CrossRef](#)]
4. Casella, D.; Dietrich, S.; Di Paola, F.; Formenton, M.; Mugnai, A.; Porcù, F.; Sanò, P. Pm-gcd—a combined ir–mw satellite technique for frequent retrieval of heavy precipitation. *Nat. Hazards Earth Syst. Sci.* **2012**, *12*, 231–240. [[CrossRef](#)]
5. Di Paola, F.; Casella, D.; Dietrich, S.; Mugnai, A.; Ricciardelli, E.; Romano, F.; Sanò, P. Combined mw-ir precipitation evolving technique (pet) of convective rain fields. *Nat. Hazards Earth Syst. Sci.* **2012**, *12*, 3557–3570. [[CrossRef](#)]
6. Munoz, E.A.; Paola, F.D.; Lanfri, M. Advances on rain rate retrieval from satellite platforms using artificial neural networks. *IEEE Lat. Am. Trans.* **2015**, *13*, 3179–3186. [[CrossRef](#)]
7. Sanò, P.; Panegrossi, G.; Casella, D.; Di Paola, F.; Milani, L.; Mugnai, A.; Petracca, M.; Dietrich, S. The passive microwave neural network precipitation retrieval (pnpr) algorithm for amsu/mhs observations: Description and application to european case studies. *Atmos. Meas. Tech.* **2015**, *8*, 837–857. [[CrossRef](#)]
8. Goodrich, D.C.; Faurès, J.-M.; Woolhiser, D.A.; Lane, L.J.; Sorooshian, S. Measurement and analysis of small-scale convective storm rainfall variability. *J. Hydrol.* **1995**, *173*, 283–308. [[CrossRef](#)]
9. Ahmad, S.; Kalra, A.; Stephen, H. Estimating soil moisture using remote sensing data: A machine learning approach. *Adv. Water Resour.* **2010**, *33*, 69–80. [[CrossRef](#)]
10. Spracklen, D.V.; Arnold, S.R.; Taylor, C.M. Observations of increased tropical rainfall preceded by air passage over forests. *Nature* **2012**, *489*, 282–285. [[CrossRef](#)] [[PubMed](#)]
11. Song, Y.; Liu, H.; Wang, X.; Zhang, N.; Sun, J. Numerical simulation of the impact of urban non-uniformity on precipitation. *Adv. Atmos. Sci.* **2016**, *33*, 783–793. [[CrossRef](#)]
12. AghaKouchak, A.; Mehran, A.; Norouzi, H.; Behrangi, A. Systematic and random error components in satellite precipitation data sets. *Geophys. Res. Lett.* **2012**, *39*, 1–4. [[CrossRef](#)]
13. Hsu, K.-I.; Gao, X.; Sorooshian, S.; Gupta, H.V. Precipitation estimation from remotely sensed information using artificial neural networks. *J. Appl. Meteorol.* **1997**, *36*, 1176–1190. [[CrossRef](#)]
14. Huffman, G.J.; Adler, R.F.; Arkin, P.; Chang, A.; Ferraro, R.; Gruber, A.; Janowiak, J.; McNab, A.; Rudolf, B.; Schneider, U. The global precipitation climatology project (gpcp) combined precipitation dataset. *Bull. Am. Meteorol. Soc.* **1997**, *78*, 5–20. [[CrossRef](#)]
15. Huffman, G.J.; Bolvin, D.T.; Nelkin, E.J.; Wolff, D.B.; Adler, R.F.; Gu, G.; Hong, Y.; Bowman, K.P.; Stocker, E.F. The trmm multisatellite precipitation analysis (tampa): Quasi-global, multiyear, combined-sensor precipitation estimates at fine scales. *J. Hydrometeorol.* **2007**, *8*, 38–55. [[CrossRef](#)]
16. Asadullah, A.; McIntyre, N.; Kigobe, M.A.X. Evaluation of five satellite products for estimation of rainfall over uganda/evaluation de cinq produits satellitaires pour l'estimation des précipitations en ouganda. *Hydrol. Sci. J.* **2008**, *53*, 1137–1150. [[CrossRef](#)]
17. Joyce, R.J.; Janowiak, J.E.; Arkin, P.A.; Xie, P. Cmorph: A method that produces global precipitation estimates from passive microwave and infrared data at high spatial and temporal resolution. *J. Hydrometeorol.* **2004**, *5*, 287–296. [[CrossRef](#)]
18. Bennartz, R.; Schroeder, M. Convective activity over africa and the tropical atlantic inferred from 20 years of geostationary meteosat infrared observations. *J. Clim.* **2012**, *25*, 156–169. [[CrossRef](#)]
19. Iguchi, T.; Kozu, T.; Meneghini, R.; Awaka, J.; Okamoto, K. Rain-profiling algorithm for the trmm precipitation radar. *J. Appl. Meteorol. Climatol.* **1997**, *39*, 2038–2052. [[CrossRef](#)]
20. Immerzeel, W.W.; Rutten, M.M.; Droogers, P. Spatial downscaling of trmm precipitation using vegetative response on the iberian peninsula. *Remote Sens. Environ.* **2009**, *113*, 362–370. [[CrossRef](#)]
21. Jia, S.; Zhu, W.; Lú, A.; Yan, T. A statistical spatial downscaling algorithm of trmm precipitation based on ndvi and dem in the qaidam basin of China. *Remote Sens. Environ.* **2011**, *115*, 3069–3079. [[CrossRef](#)]

22. Xu, S.; Wu, C.; Wang, L.; Gonsamo, A.; Shen, Y.; Niu, Z. A new satellite-based monthly precipitation downscaling algorithm with non-stationary relationship between precipitation and land surface characteristics. *Remote Sens. Environ.* **2015**, *162*, 119–140. [[CrossRef](#)]
23. Chen, C.; Zhao, S.; Duan, Z.; Qin, Z. An improved spatial downscaling procedure for trmm 3b43 precipitation product using geographically weighted regression. *IEEE J. Sel. Top. Appl. Earth Obs. Remote Sens.* **2015**, *8*, 4592–4604. [[CrossRef](#)]
24. Cui, Y.; Long, D.; Hong, Y.; Zeng, C.; Zhou, J.; Han, Z.; Liu, R.; Wan, W. Validation and reconstruction of fy-3b/mwri soil moisture using an artificial neural network based on reconstructed modis optical products over the tibetan plateau. *J. Hydrol.* **2016**, *543*, 242–254. [[CrossRef](#)]
25. Coulibaly, P.; Evora, N.D. Comparison of neural network methods for infilling missing daily weather records. *J. Hydrol.* **2007**, *341*, 27–41. [[CrossRef](#)]
26. Long, D.; Shen, Y.; Sun, A.; Hong, Y.; Longuevergne, L.; Yang, Y.; Li, B.; Chen, L. Drought and flood monitoring for a large karst plateau in southwest China using extended grace data. *Remote Sens. Environ.* **2014**, *155*, 145–160. [[CrossRef](#)]
27. Peng, J.; Loew, A.; Merlin, O.; Verhoest, N.E.C. A review of spatial downscaling of satellite remotely sensed soil moisture. *Rev. Geophys.* **2017**, *55*, 341–366. [[CrossRef](#)]
28. Gislason, P.O.; Benediktsson, J.A.; Sveinsson, J.R. Random forests for land cover classification. *Pattern Recognit. Lett.* **2006**, *27*, 294–300. [[CrossRef](#)]
29. Xu, X.; Lu, C.; Shi, X.; Ding, Y. Large-scale topography of China: A factor for the seasonal progression of the meiyu rainband? *J. Geophys. Res.* **2010**, *115*. [[CrossRef](#)]
30. Yang, F.; Lau, K.M. Trend and variability of China precipitation in spring and summer: Linkage to sea-surface temperatures. *Int. J. Climatol.* **2004**, *24*, 1625–1644. [[CrossRef](#)]
31. Barbosa, H.A.; Huete, A.R.; Baethgen, W.E. A 20-year study of ndvi variability over the northeast region of brazil. *J. Arid Environ.* **2006**, *67*, 288–307. [[CrossRef](#)]
32. Barbosa, H.A.; Lakshmi Kumar, T.V. Influence of rainfall variability on the vegetation dynamics over northeastern brazil. *J. Arid Environ.* **2016**, *124*, 377–387. [[CrossRef](#)]
33. Cihlar, J.; St-Laurent, L.; Dyer, J.A. Relation between the normalized difference vegetation index and ecological variables. *Remote Sens. Environ.* **1991**, *35*, 279–298. [[CrossRef](#)]
34. Ding, M.; Zhang, Y.; Liu, L.; Zhang, W.; Wang, Z.; Bai, W. The relationship between ndvi and precipitation on the tibetan plateau. *J. Geograph. Sci.* **2007**, *17*, 259–268. [[CrossRef](#)]
35. Jingyong, Z.; Wenjie, D.; Congbin, F.; Lingyun, W. The influence of vegetation cover on summer precipitation in China: A statistical analysis of ndvi and climate data. *Adv. Atmos. Sci.* **2003**, *20*, 1002–1006. [[CrossRef](#)]
36. Breiman, L. Random forests. *Mach. Learn.* **2001**, *45*, 5–32. [[CrossRef](#)]
37. Breiman, L.; Friedman, J.H.; Olshen, R.A.; Stone, C.J. *Classification Regression Trees*; Chapman and Hall/CRC: Boca Raton, FL, USA, 1984.
38. Deng, J. Some problems on the comprehensive agricultural regionalization of China. *Geogr. Res.* **1982**, *1*, 9–18.
39. Zhou, L.; Sun, H.; Shen, Y.; Deng, J.; Shi, Y. Comprehensive agricultural planning of China. *Chin. Agric.* **1981**, *21*.
40. Zhang, X.; Friedl, M.A.; Schaaf, C.B.; Strahler, A.H.; Liu, Z. Monitoring the response of vegetation phenology to precipitation in africa by coupling modis and trmm instruments. *J. Geophys. Res. Atmos.* **2005**, *110*, 1545–1555. [[CrossRef](#)]
41. Wang, J.; Price, K.P.; Rich, P.M. Spatial patterns of ndvi in response to precipitation and temperature in the central great plains. *Int. J. Remote Sens.* **2001**, *22*, 3827–3844. [[CrossRef](#)]
42. Vicente-Serrano, S.M.; Gouveia, C.; Camarero, J.J.; Beguería, S.; Trigo, R.; López-Moreno, J.I.; Azorín-Molina, C.; Pasho, E.; Lorenzo-Lacruz, J.; Revuelto, J.; et al. Response of vegetation to drought time-scales across global land biomes. *Proc. Natl. Acad. Sci. USA* **2013**, *110*, 52–57. [[CrossRef](#)] [[PubMed](#)]
43. Zhong, L.; Ma, Y.; Salama, M.S.; Su, Z. Assessment of vegetation dynamics and their response to variations in precipitation and temperature in the tibetan plateau. *Clim. Chang.* **2010**, *103*, 519–535. [[CrossRef](#)]
44. Guan, H.; Wilson, J.L.; Xie, H. A cluster-optimizing regression-based approach for precipitation spatial downscaling in mountainous terrain. *J. Hydrol.* **2009**, *375*, 578–588. [[CrossRef](#)]

45. Yin, Z.-Y.; Zhang, X.; Liu, X.; Colella, M.; Chen, X. An assessment of the biases of satellite rainfall estimates over the tibetan plateau and correction methods based on topographic analysis. *J. Hydrometeorol.* **2008**, *9*, 301–326. [[CrossRef](#)]
46. Sokol, Z.; Bližňák, V. Areal distribution and precipitation–altitude relationship of heavy short-term precipitation in the czech republic in the warm part of the year. *Atmos. Res.* **2009**, *94*, 652–662. [[CrossRef](#)]
47. Kang, S.; Xu, Y.; You, Q.; Flügel, W.-A.; Pepin, N.; Yao, T. Review of climate and cryospheric change in the tibetan plateau. *Environ. Res. Lett.* **2010**, *5*, 015101. [[CrossRef](#)]
48. You, Q.; Kang, S.; Aguilar, E.; Yan, Y. Changes in daily climate extremes in the eastern and central tibetan plateau during 1961–2005. *J. Geophys. Res.* **2008**, *113*, 1639–1647. [[CrossRef](#)]



© 2017 by the authors. Licensee MDPI, Basel, Switzerland. This article is an open access article distributed under the terms and conditions of the Creative Commons Attribution (CC BY) license (<http://creativecommons.org/licenses/by/4.0/>).